# Icosahedral Short-Range Order in Amorphous Alloys

W. K. Luo,[1] H.W. Sheng,[1] F. M. Alamgir,[2] J. M. Bai,[3] J. H. He,[1] and E. Ma[1,*]

[1]*Department of Materials Science and Engineering, The Johns Hopkins University, Baltimore, Maryland 21218, USA*
[2]*Brookhaven National Laboratory, Upton, New York 11973, USA*
[3]*High-Temperature Materials Lab, Oak Ridge National Laboratory, Oak Ridge, Tennessee 37831, USA*

(Received 2 October 2002; published 8 April 2004)

We have characterized the icosahedral short-range order in amorphous solids using local environment probes. Such topological local order is pronounced even in an amorphous alloy that does *not* form quasicrystalline phases upon crystallization, as demonstrated by the extended x-ray absorption fine structure and x-ray absorption near-edge structure of a Ni-Ag amorphous alloy analyzed through reverse Monte Carlo simulations.

DOI: 10.1103/PhysRevLett.92.145502 PACS numbers: 61.25.Mv, 61.20.Ja, 61.43.–j, 64.60.My

The nature of the short-range structure of metallic liquids and glasses is of fundamental interest [1–4], but is much less understood than the well-defined crystalline structures. Icosahedral clusters have been proposed to be an important building block, according to the polytetrahedral model of amorphous phases [2,3]. However, our knowledge of such icosahedral short-range order (ISRO) has relied heavily on computer simulations based on empirical potentials [3,5–8], because it is rather difficult, if not impossible, to directly image the short-range arrangement of atoms or local fivefold symmetry [4,9].

Recently, direct experimental evidence for the presence of fivefold symmetry has been obtained in liquid Pb [10]. There are also some very recent neutron scattering data [11] that suggest ISRO in undercooled elemental metallic melts. For metallic amorphous *solids*, the study of ISRO has normally been carried out in alloys because amorphous pure metals are not available [12]. While the use of alloys naturally brings in chemical ordering that may enhance or disfavor ISRO, the latter has been believed to be present. However, *direct* experimental evidence has not been forthcoming. For some quasicrystal forming systems such as those based on Al or Zr [13–20], x-ray, neutron, or electron scattering data and the pair distribution functions derived therefrom, or other spectroscopy and kinetics data, have been compared between the icosahedrally coordinated quasicrystalline phase and the parent amorphous alloy (or undercooled liquid). The common features observed are taken as the proof, albeit indirect, that the fivefold symmetry also exists over short to medium range in the amorphous phases. Recently, ordered regions in amorphous alloys were found using transmission electron microscopy (TEM) [9,20]. But all this evidence indicating ISRO may well be attributable to the embryos of the quasicystalline phases. This is especially true for the relatively large ($> \sim 2$ nm) icosahedral regions observed under TEM [20], which almost certainly are the (quenched-in) nuclei of the quasicrystals.

It is, therefore, of interest to establish if the ISRO can be an intrinsic and prevalent feature, by *quantitatively* examining the degree of its development in an amorphous alloy from which *no* quasicrystalline phase evolves. In this study, we examine a Ni-Ag amorphous alloy [21,22], which is interesting because it directly crystallizes into a mixture of fcc Ni and Ag with no (intermediate) quasicrystals. In fact, there is no known equilibrium or metastable compound in this system at all and hence no competing crystallinelike local environment other than the close-packed fcc order. Complications from complex chemical order that often dominate in glass-forming systems with a large negative heat of mixing [23] are therefore avoided. Also, our recent molecular dynamics (MD) simulations predicted that amorphous Ni-Ag would develop strong ISRO, increasing with undercooling, even at very high effective quench rates [22]. We report in this Letter the determination of the ISRO using local environment probes, extended x-ray absorption fine structure (EXAFS) and x-ray absorption near-edge structure (XANES), through an analysis employing the reverse Monte Carlo (RMC) method.

$Ni_{60}Ag_{40}$ foils with thickness up to 5 $\mu$m were prepared using dc sputter deposition of a composite target onto liquid nitrogen cooled Si substrates [21]. TEM, differential scanning calorimetry (DSC), and magnetic property measurements all confirmed that an amorphous alloy was obtained [21,24]. Transmission Ni *K*-edge and Ag *K*-edge EXAFS data, and x-ray diffraction (XRD) data, were collected at beam line X23A2 and X14A, respectively, of NSLS at BNL. The EXAFS spectra were Fourier transformed (FT) shown in the upper panel of Fig. 1, and the first peak corresponding to the first coordination shell was then inverse-Fourier transformed (IFT) to obtain the *k*-space spectra, shown in the lower panel of Fig. 1.

Three-dimensional atomic configuration of the amorphous $Ni_{60}Ag_{40}$ is constructed using RMC [25] simulations of the EXAFS, as well as the XRD spectrum in Fig. 1. The advantage of this method is that it provides atomic positions, through statistical matches between theoretical and experimental spectra under constraints,

  

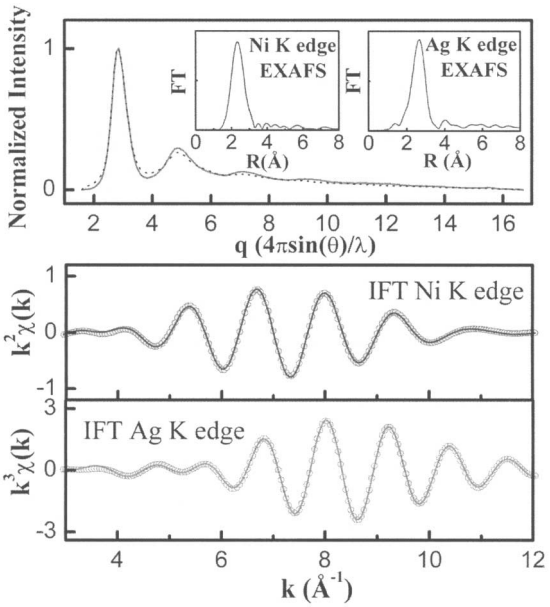


FIG. 1. Upper panel: Solid lines are the experimental XRD and Fourier-transformed (FT) EXAFS data for the $Ni_{60}Ag_{40}$ amorphous alloy. The dashed line is the RMC simulated XRD. Lower panel: the solid lines present the inverse Fourier transforms (IFT) of the first peaks in the FT EXAFS spectra, in comparison with the RMC simulation (circles).

directly from experimental data without any hypothetical structural model. As a result, it avoids the traditional structural search by trial and error, where the features observed in radial distribution functions (RDF) or structure factor obtained from scattering data are compared with model predictions based on *assumed* packing geometries [23,26,27]. The 1D scattering data also have an inherent limitation in their ability to discriminate among various models, as they only provide information about average atomic pair separations and coordination numbers, with no information about the bond angles and 3D atomic positions (sometimes not even about partial pair correlations). In comparison, EXAFS is element specific so that we can examine the surroundings of each species from multiple edges. With the RMC, the information drawn from the experiments can then be boosted from one to three dimensions [28].

Multiple spectra can be simultaneously used for RMC to provide more constraints on the statistical sampling of the topological arrangements. We used both the Ni $K$-edge and Ag $K$-edge EXAFS, as well as the XRD pattern because, while EXAFS is sensitive to the local environment, the XRD pattern adds information beyond the nearest neighbors and about the density of the system. A random atomic configuration in a cubic box (side length of 38.5 nm) of 4 000 atoms was constructed for $Ni_{60}Ag_{40}$ with periodic boundary conditions. The scale of the simulation box was determined by the XRD and the closest distance between the atoms was based on the partial RDFs from MD simulation [22]. An atomic guess configuration is generated by randomly moving or exchanging atoms. The structure is improved by reducing the normalized fit residual, $\delta^2$, between the simulated ($\chi_{\text{simul}}$) and experimental ($\chi_{\text{exp}}$) spectra

$$\delta^2 = \frac{\sum_i \{k_i^n [\chi_{\text{simul}}(k_i) - \chi_{\text{exp}}(k_i)]\}^2}{\sigma^2 \sum_i [k_i^n \chi_{\text{exp}}(k_i)]^2}, \quad (1)$$

where $\sigma$ is an error and the $k$ weighting factor $n$ are taken as 2, 3, and 0 for the Ni $K$-edge, Ag $K$-edge EXAFS, and XRD pattern, respectively. The $\delta^2$s for the three spectra are assumed to be additive, with weighting factors 0.3, 0.2, and 0.5, respectively, which, together with $n$, control the relative contribution of each spectrum to the overall RMC fitting. The choice of such weighting is based on the quality of the EXAFS data at the two edges, as well as the high signal-to-noise ratio of the XRD data taken with the synchrotron light source. The RMC simulation is implemented using the Metropolis algorithm and the experimental spectra as the potential in lieu of a force field. The error $\sigma$ served as "temperature" and was slowly "cooled" from 10 to $10^{-3}$ following the simulated annealing scheme [29]. Using the atomic positions in the configuration, the EXAFS was calculated in the single scattering approximation [30], with the amplitude and phase shift obtained from the *ab initio* FEFF8 code [31]. The real energy shifts for various scattering paths were optimized in the fitting. The XRD pattern was calculated using the Debye scattering formula [32].

The eventual matches between the RMC simulated and the experimental spectra after $\sim 10^7$ RMC steps are demonstrated in Fig. 1. Although the RMC solution may not be unique, the configuration obtained passed the following two major checks. First, in comparison with an MD simulation of the Ni-Ag liquid quenched to below glass transition [22], the RMC configuration yielded not only a similar chemical short-range order parameter (0.27), but also similar RDFs (see the inset in Fig. 3). The enthalpy of the simulated structure agrees with the DSC value as well [21]. Note that the MD simulation employed embedded atom method potentials and had no input from the x-ray experiments.

Second, the RMC configuration was further justified by calculating its XANES and comparing with experimental data. While the single scattering of EXAFS is associated with pair correlations, the multiple scattering in XANES confers the sensitivity to higher-order correlation functions and is hence capable of providing information about the geometrical arrangement of the absorbing and neighboring atoms not dominant in EXAFS or standard diffraction data [33]. A precise reproduction of all XANES features using *ab initio* calculations is not always attainable, which, together with the extensive calculations required for multiple scattering in relatively large

clusters, precludes a direct RMC simulation of XANES. However, a FEFF8 [31] calculation of the XANES provides a useful check of the final RMC configuration and helps explain which bonding orbitals or structural characteristics give rise to certain XANES features. Multiple scattering path expansion was performed on each atom in the simulation box for clusters of a radius around 10 Å (>150 atoms). To compare with experimental XANES, we have considered the broadening due to the core hole lifetime, the finite mean free path of the photoelectron, and the experimental resolution. Figure 2(a) demonstrates that the features in the calculated spectrum match those in the measured Ni *K*-edge XANES. These XANES features are also obviously different from the double-peak feature of both the fcc Ni and hypothetical fcc Ni-Ag clusters. A match was achieved as well between the Ag-edge XANES measured for the alloy and that calculated for the RMC configuration, Fig. 2(b). Therefore, the RMC amorphous configuration produces not only the correct EXAFS and XRD, but also the right XANES, and fcc clusters can be ruled out as the dominant building blocks.

The RMC configuration shows a coordination number distribution from 9 to 16, with an average of 12.6. The topological SRO is analyzed using the common-neighbor (CN) analysis [6] that decomposes the first RDF peak according to the different local environment of the bonded nearest neighbor (N-N) pairs (i.e., those within a cutoff distance corresponding to the first minimum of the total RDF shown in the inset of Fig. 3). Each bonded pair of atoms is classified according to its surroundings using a set of three indices, *jkl*. The first index *j* is the number of N-N's common to both atoms. The second index *k* specifies the number of N-N bonds between the *j* CN atoms themselves. The third index *l* is the number of bonds in the longest continuous chain formed by the *k* CN bonds. The CN analysis can distinguish between the fcc [34], hcp, and icosahedral packing and is more sensitive to local order than the bond spherical harmonics method [35]. Specifically, all bonded pairs in an icosahedron of 13 atoms are of type 555, e.g., the central atom forms a 555 pair with each of its 12 neighbors. If one bond is broken between a pair of outer atoms in an icosahedron, two of the 555 pairs are transformed into 544 and two into 433 pairs [5,6]. In contrast, the fcc packing has the 421 type only, while the hcp has equal numbers of 421 and 422 [6]. The relative fractions of the major pairs types (others negligible) in the RMC configuration are shown in the histogram of Fig. 3. The most abundant pairs are 555, 433, and 544, indicating the dominance of icosahedral packing. The high fractions of distorted icosahedral order (544 and 433) are not surprising for the highly nonequilibrium deposition conditions where kinetics are severely limited for organizing the five-member rings. Only small percentages of 422 and 421 pairs are found, indicating insignificant hcp and fcc local orders. The middle inset in Fig. 3 shows the 48 perfect icosahedra in the RMC box. The centers of the icosahedral cages are almost always the smaller Ni atoms, surrounded by 12 (Ni + Ag) atoms [7,22].

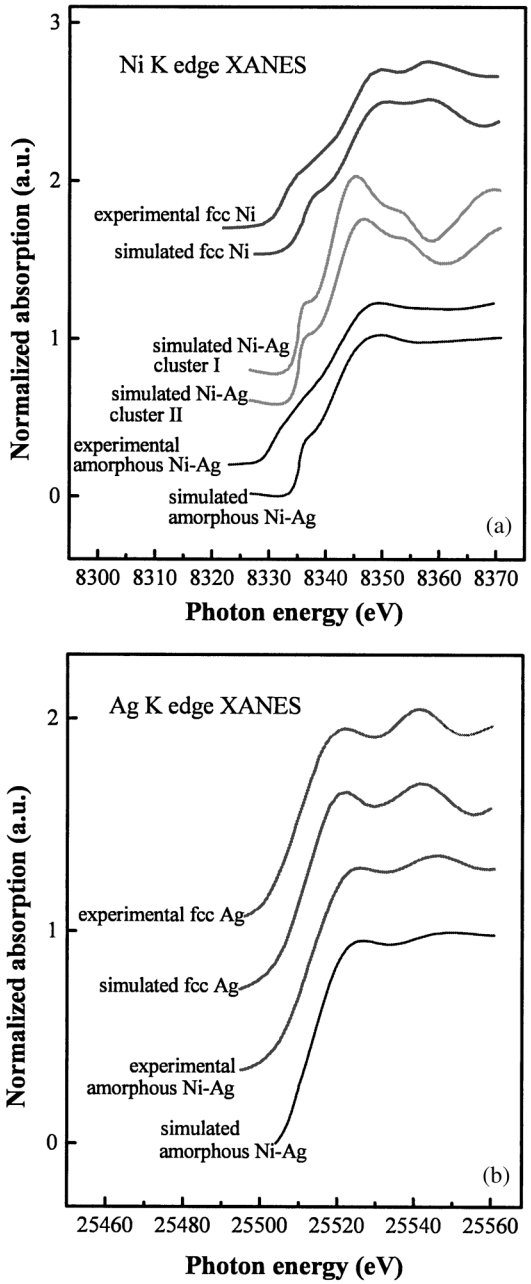


FIG. 2. Ni *K*-edge (a) and Ag *K*-edge (b) XANES spectra calculated for Ni (or Ag) in the RMC-simulated amorphous $Ni_{60}Ag_{40}$. The calculations averaged XANES of 2400 Ni-centered clusters and 1600 Ag-centered clusters, respectively, within the RMC configuration. The XANES features are consistent with those measured of the $Ni_{60}Ag_{40}$ amorphous alloy, but different from those of experimental or simulated fcc bulk Ni (or Ag), and from those calculated for artificially constructed ordered Ni-Ag fcc clusters (cluster I for $L1_0$ and cluster II for $L1_2$).

In conclusion, systematic EXAFS, XANES, and XRD experiments in combination with the RMC modeling

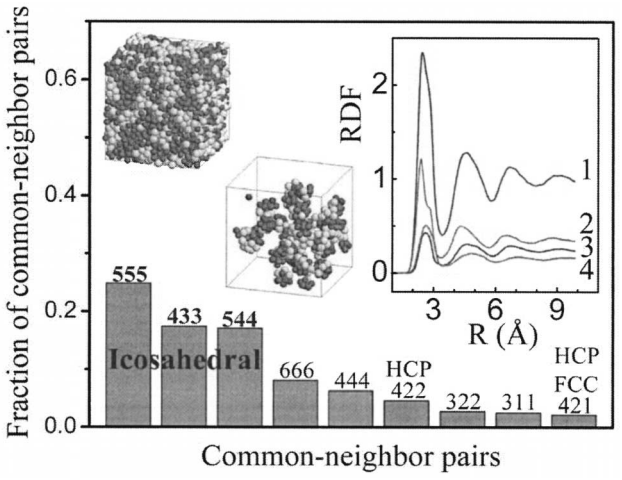


FIG. 3. Normalized common-neighbor pairs of the $Ni_{60}Ag_{40}$ amorphous alloy. The insets show the 3D RMC configuration, and its total (line 1) and partial RDFs (lines 2 to 4 for Ni-Ni, Ni-Ag or Ag-Ni, and Ag-Ag, respectively, weighted by their contributions to the total RDF), as well as the 48 *perfect* icosahedra (the center atom forms twelve 555 pairs with the neighbors), involving 13% of the atoms. The dark spheres are Ni atoms.

demonstrate that ISRO develops in amorphous $Ni_{60}Ag_{40}$ to a very high degree, even though the Ni-Ag system has no tendency to form quasicrystals. Such short-range topological arrangements require only limited diffusion and hence develop despite of severe kinetic constraints, in agreement with MD predictions [22]. At large undercooling to low temperatures, the increased ISRO contributes to enthalpy reduction by promoting the dense packing that maximizes the number of bonds, as shown in previous energy calculations [3,7]. The predominance of the ISRO over the close-packed character [3] can be viewed as a proof for the metastable and amorphous nature of the alloy: in transforming to crystals, atoms have to break their local symmetry and reorganize at the amorphous-crystal interface to produce the translationally invariant network compatible with crystals. This renders crystallization a first-order transition, as seen in the isothermal DSC experiment [21,36].

This work is supported by DoE under DE-FG02-03ER46056. Beam line X14A at NSLS is part of the HTML User Program, ORNL, under DoE Contract No. DE-AC05-00OR22725.

*Corresponding author; electronic address: ema@jhu.edu

[1] F. C. Frank, Proc. R. Soc. London A **215**, 43 (1952).
[2] D. R. Nelson and F. Spaepen, Solid State Phys. Adv. Res. Appl. **42**, 1 (1989).
[3] J. P. K. Doye and D. J. Wales, Science **271**, 484 (1996).
[4] F. Spaepen, Nature (London) **408**, 781 (2000).
[5] H. Jónsson and H. C. Anderson, Phys. Rev. Lett. **60**, 2295 (1988).
[6] A. S. Clarke and H. Jónsson, Phys. Rev. E **47**, 3975 (1993).
[7] S. Cozzini and M. Ronchetti, Phys. Rev. B **53**, 12 040 (1996).
[8] F. Yonezawa, Solid State Phys. **45**, 179 (1991).
[9] T. Takagi *et al.*, Appl. Phys. Lett. **79**, 485 (2001).
[10] H. Reichert *et al.*, Nature (London) **408**, 839 (2000).
[11] T. Schenk *et al.*, Phys. Rev. Lett. **89**, 075507 (2002).
[12] J.-M. Dubois, F. Montoya, and C. Back, Mater. Sci. Eng. **A178**, 285 (1994).
[13] L. Zhang *et al.*, J. Non-Cryst. Solids **262**, 169 (2000).
[14] M. W. Chen *et al.*, Appl. Phys. Lett. **79**, 42 (2001).
[15] L. Q. Xing *et al.*, Appl. Phys. Lett. **77**, 1970 (2000).
[16] D. Shechtman, I. Blech, D. Gratias, and J. W. Cahn, Phys. Rev. Lett. **53**, 1951 (1984).
[17] D. D. Kofalt, S. Nanao, T. Egami, K. M. Wong, and S. J. Poon, Phys. Rev. Lett. **57**, 114 (1986).
[18] L. E. Levine, P. C. Gibbons, and K. F. Kelton, Phys. Rev. B **40**, 9338 (1989).
[19] C. H. Chen, D. C. Joy, H. S. Chen, and J. J. Hauser, Phys. Rev. Lett. **57**, 743 (1986).
[20] J. Saida, M. Matsushita, and A. Inoue, Appl. Phys. Lett. **79**, 412 (2001).
[21] J. H. He, H. W. Sheng, P. J. Schilling, C.-L. Chien, and E. Ma, Phys. Rev. Lett. **86**, 2826 (2001).
[22] J. H. He and E. Ma, Phys. Rev. B **64**, 144206 (2001).
[23] G. S. Cargill, J. Appl. Phys. **41**, 2248 (1970).
[24] L. Sun, J. H. He, H. W. Sheng, P. C. Searson, C.-L. Chien, and E. Ma, J. Non-Cryst. Solids **317**, 164 (2003).
[25] S. J. Gurman and R. L. McGreevy, J. Phys. Condens. Matter **2**, 9463 (1990).
[26] T. Egami, W. Dmowski, Y. He, and R. B. Schwarz, Metall. Mater. Trans. A **29**, 1805 (1998).
[27] N. Mattern *et al.*, Acta Mater. **50**, 305 (2002).
[28] J. Hafner, J. Non-Cryst. Solids **205–207**, 934 (1996).
[29] W. H. Press *et al.*, *Numerical Recipes in FORTRAN 90* (Cambridge University Press, Cambridge, 1996).
[30] A. Filiponi, J. Phys. Condens. Matter **6**, 8415 (1994).
[31] A. L. Ankudinov, B. Ravel, J. J. Rehr, and S. D. Conradson, Phys. Rev. B **58**, 7565 (1998).
[32] V. Rosato and M. Celino, J. Appl. Phys. **86**, 6826 (1999).
[33] A. Bianconi, in *X-Ray Absorption: Principles, Applications, Techniques of EXAFS, SEXAFS, and XANES*, edited by D. C. K. Koningsberger and R. Prins (Wiley, New York, 1988), Vol. 92, p. 573.
[34] H. W. Sheng, J. H. He, and E. Ma, Phys. Rev. B **65**, 184203 (2002).
[35] P. J. Steinhardt, D. R. Nelson, and M. Ronchetti, Phys. Rev. B **28**, 784 (1983).
[36] L. C. Chen and F. Spaepen, Nature (London) **336**, 366 (1988).